



# **Experimental Study on the Critical-State and Energy Dissipation Behaviors of Rubber-Sand Mixtures**

Beibing Dai<sup>1</sup>; Yiyuan Chen<sup>2</sup>; Dan Chang<sup>3</sup>; Jun Yang, F.ASCE<sup>4</sup>; and Jiankun Liu<sup>5</sup>

**Abstract:** In the present study, a number of triaxial tests were conducted to examine the shear behavior of rubber–sand mixtures, with an emphasis placed on the critical-state line and energy performance. The experimental results indicated that under otherwise similar conditions, the deviatoric stress reduces with increasing rubber content but increases with increasing confining pressure. The promotion of confining pressure and rubber content contributed to increased contractiveness of rubber–sand mixtures (RSM) in shear. The position of the critical-state line (CSL) in the e-lnp' plane depended on both rubber content and confining pressure, and it shifted toward the right (or upward) direction with an increase of confining pressure and rotated in a clockwise direction with an increase of rubber content. The slope of the critical-state line (M) in the q-p' plane decreased as the rubber content increased. In addition, the energy analysis indicated that most work input is dissipated, with the stored elastic potential energy taking a minor proportion. The energy dissipation decreased with increasing rubber content and increased with increasing consolidation pressure. Macroscopically, this was associated with the stress level within a specimen and microscopically linked with the contact force level and related energy dissipation through the interparticle friction behaviors. **DOI:** 10.1061/IJGNALGMENG-8818. © 2023 American Society of Civil Engineers.

Author keywords: Rubber-sand mixture; Shear behavior; Critical-state line; Energy dissipation.

#### Introduction

With the rapid development of the automobile industry in recent years, the increasing waste tire rubber has caused a detrimental effect on the natural environment and aroused wide public concern since rubber is a material that is flammable and not easily biodegradable. However, on account of the attributes of light specific weight, high damping capacity, and good deformability (Humphrey 1999; Garga and O'Shaughnessy 2000; Cheng et al. 2020), the waste tire rubber can be recycled for the production of rubber–soil mixtures that have a wide spectrum of geotechnical applications such as filling materials in embankments or behind retaining walls, seismic isolation in building foundations, and reinforcement materials for slope stabilization (Bosscher et al. 1997; Lee et al. 1999; Tsang et al. 2012). Owing to the discrete nature of the mixture and the presence of soft rubber particles, the rubber–soil mixtures exhibit rather complex mechanical behaviors

Note. This manuscript was submitted on January 22, 2023; approved on August 23, 2023; published online on December 27, 2023. Discussion period open until May 27, 2024; separate discussions must be submitted for individual papers. This paper is part of the *International Journal of Geomechanics*, © ASCE, ISSN 1532-3641.

(Zornberg et al. 2004; Bergado et al. 2005; Pistolas et al. 2018), which cannot easily be captured by traditional continuum mechanics approach (Alimirzaei et al. 2019; Kumar et al. 2021; Katiyar et al. 2022). Thus, there is an urgent need to study their strength and deformation behaviors in detail.

A number of studies have shown that that the mechanical properties of rubber-soil mixtures are affected by the rubber content, particle size, relative density and consolidation pressure, and so on (Lopera Perez et al. 2016; Asadi et al. 2018; Shariatmadari et al. 2018; Liu et al. 2018; Li et al. 2019; Senthen Amuthan et al. 2020; Ding et al. 2021; Wu et al. 2021; Fakharian and Ahmad 2021; Dai et al. 2023; Wu et al. 2023). For example, Fuchiyama et al. (2015) carried out the triaxial tests on the rubber-soil mixtures by focusing on the influence of rubber particle size and observed that a specimen with a smaller rubber particle size tends to achieve a larger residual strain. Through the performance of a number of direct shear tests, Anvari et al. (2017) revealed that the addition of rubber particles promotes the shear strength of sands in loose and medium-dense states. Shariatmadari et al. (2018) conducted hollow cylinder tests and found that the shear strength of rubber-soil mixtures increases with increasing rubber content. However, the experimental results obtained by Tabrizi et al. (2019) indicated that the impact of rubber content on the shear strength of rubber-soil mixtures depends on the consolidation stress level. On the basis of a series of dynamic hollow cylinder tests, Sarajpoor et al. (2020) concluded that the dynamic properties of rubber-soil mixtures are mainly influenced by the confining pressure and rubber content but are less dependent on the rubber particle size and relative density.

In particular, the critical-state shearing and dynamic damping performance of granular soils play an important role in a wide range of geotechnical applications (Yang and Luo 2018). The particle attributes such as interparticle friction and particle size are important factors affecting the shear behavior of granular materials at the critical state (Gu et al. 2014; Dai et al. 2016; Dai 2018). A number of researchers have done experiments and numerical simulations to explore the critical-state shear behaviors of rubber–soil

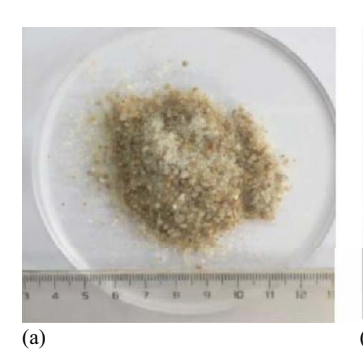
<sup>&</sup>lt;sup>1</sup>Associate Professor, School of Civil Engineering, Sun Yat-sen Univ., Guangzhou 510275, China. ORCID: https://orcid.org/0000-0002-5924-2130. Email: daibb@mail.sysu.edu.cn

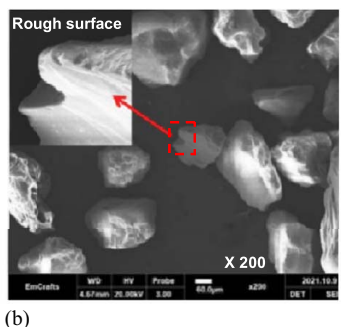
<sup>&</sup>lt;sup>2</sup>Master's Student, School of Civil Engineering, Sun Yat-sen Univ., Guangzhou 510275, China. Email: 794468258@qq.com

<sup>&</sup>lt;sup>3</sup>Associate Professor, School of Civil Engineering, Sun Yat-sen Univ., Guangzhou 510275, China; Southern Marine Science and Engineering Guangdong Laboratory (Zhuhai), Zhuhai 519082, China (corresponding author). Email: changd@mail.sysu.edu.cn

<sup>&</sup>lt;sup>4</sup>Professor, Dept. of Civil Engineering, Univ. of Hong Kong, Hong Kong, China. Email: junyang@hku.hk

<sup>&</sup>lt;sup>5</sup>Professor, School of Civil Engineering, Sun Yat-sen Univ., Guang-zhou 510275, China; Southern Marine Science and Engineering Guang-dong Laboratory (Zhuhai), Zhuhai 519082, China. Email: liujiank@mail.sysu.edu.cn







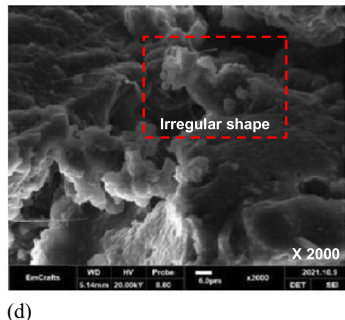


**Fig. 1.** Images of sand and rubber particles: (a) sand particles; (b) SEM photos for sand particles; (c) rubber particles; and (d) SEM photos for rubber particles.

mixtures (Fu et al. 2014; Lopera Perez et al. 2017; Indraratna et al. 2019). Fu et al. (2017) observed through the triaxial tests that the critical-state line (CSL) in the e-lnp' plane rotates around a certain pivot point as the rubber content increases and that the rubber particle size exerts a significant impact on the critical-state line as well. Compared with traditional sands, rubber-soil mixtures have much higher compressibility, which makes it difficult for them to reach the critical state in the laboratory triaxial test (Lee et al. 1999; Qi et al. 2019). Typically, a large shear strain is required for a rubber-soil mixture to achieve the critical state. In particular, the influence of the end restraint and flexible membrane on the specimen cannot be ignored (Cheung and O'Sullivan 2008; Muraro and Jommi 2019), and thus the numerical simulation method, such as the discrete element method (DEM) has been adopted to study the critical-state mechanical properties of rubber-soil mixtures. Fu et al. (2023) examined the micromechanical behaviors of rubber-soil mixtures by DEM and found that the samples with a rubber content of 20% show a continuous strain hardening behavior until the critical state is reached at more than 40% axial strain. Based on the numerical approach, Zhang et al. (2023) pointed out that an increase of rubber content results in a decrease of shear strength of rubber-soil mixtures at the critical state; they also revealed a good linear relationship between the deviatoric stress q and the mean effective stress p' at the critical state, as well as between the void ratio e and the lnp'. Bernal-Sanchez et al. (2018) found that adding rubber particles helps improve the damping capacity of sands considerably and considered that this improvement was attributed to the good deformability of rubber particles and high interparticle friction resistance. However, Nakhaei et al. (2012) obtained a different test result that the damping ratio of rubbersoil mixtures reduces with an increase of rubber content at a low confining pressure (e.g., 50 kPa) but increases at a relatively high pressure (e.g., 200 and 300 kPa). The studies of Li et al. (2016) showed that relatively large rubber particles tend to enhance the damping ratio of rubber-soil mixtures at a low confining pressure, but the particle size effect is insignificant at a high confining pressure. In addition, Fonseca et al. (2019) did a series of onedimensional consolidation tests to analyze the energy dissipation behavior of rubber-soil mixtures, finding that the energy was consumed mainly by means of the interparticle friction behaviors at the early stage of loading.

It is clear that the complex mechanical behaviors and properties of rubber—soil mixtures have been of longstanding interest to the researchers and practitioners in the community of geotechnical engineering, and a number of studies have been conducted to investigate the mechanical behaviors of rubber—soil mixtures in recent years, which provides the guidance for their engineering applications. However, a number of tricky issues, such as the critical-state

characteristics, which play an important role in the constitutive behavior of granular materials, have not been fully understood. The rubber–soil mixture is also used as a filling material owing to its good energy dissipation performance, but little research has been done to explore the energy evolution characteristics of rubber–soil mixture subjected to the shear loading. In this study, a series of triaxial tests in undrained conditions have been performed on the rubber–sand mixtures considering different confining pressures, initial packing densities, and rubber content. In particular, the critical-state shear performances and energy states of rubber–sand samples are analyzed in detail. It is hoped that the current study can shed some light on the critical-state shear behaviors and energy dissipation characteristics of rubber–sand mixtures.

## **Materials and Test Programs**

China ISO standard sand-Fujian sand was used in this experimental study. The specific weight of sand particles was 2.65. The images of sand particles are shown in Fig. 1. The particle size distribution curve is given in Fig. 2. The rubber material was commercially purchased, with the macro and micro views given in Fig. 1 and the grading curve presented in Fig. 2. Similar particle gradations were adopted for the sand and rubber particles to isolate the effect of particle size. The specific weight of rubber particles was 1.61. It is seen in Fig. 2 that the sizes of the sand and rubber particles are comparable to each other.

All samples in the triaxial tests were prepared by the dry tamping method. The *B*-value was ensured to be above 95%. Four confining pressures (i.e.,  $\sigma_r = 50$ , 100, 200, and 300 kPa) were adopted in the consolidation process. Three relative densities (i.e.,  $D_r = 100$ )

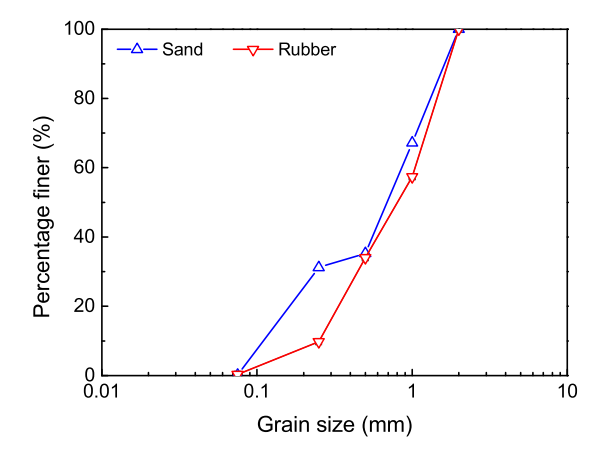


Fig. 2. Particle size distribution curves for sand and rubber particles.

Table 1. Maximum and minimum void ratios of rubber-sand mixtures

Specimen type	Maximum void ratio $e_{max}$	Minimum void ratio $e_{\min}$
Pure sand	0.723	0.364
RC = 5%	0.991	0.536
RC = 10%	1.175	0.673
RC = 15%	1.287	0.870
RC = 20%	1.668	1.034

30%, 50%, and 70%) and five types of rubber content (i.e., RC = 0%, 5%, 10%, 15%, and 20%) defined by the mass fraction of rubber particles were considered in this study. The minimum rubber content of the mixture considered in this study was 5%, which is reasonable from the point of practice and also adequately low. The maximum and minimum void ratios of the rubber–sand mixtures at various rubber contents are listed in Table 1. Thus, there were in total 60 tests, which were performed in the undrained condition. The axial loading rate was 0.4 mm/min. Note that the rubber–sand mixture is shortened as rubber–sand mixtures (RSM) in the following parts.

#### **Shear Behaviors and Critical States**

#### Shear Behaviors

Fig. 3 compares the shear behaviors of RSM samples under different confining pressures. The deviatoric stress q increases

monotoncially with the axial strain  $\varepsilon_1$  at the early shearing stage, and the specimens at  $\sigma_r = 50$  and 200 kPa seem to have arrived at a stable state at large shear strains. It is evident that increasing confining pressure contributes to an increase of deviatoric stress. Fig. 3(b) shows that, as the axial strain increases, the excess porewater pressure u for all concerned specimens increases first and decreases afterward. It is indicated that they contract at first and then dilate as the shearing proceeds. The initial contraction degree is positively correlated with the consolidation pressure level. The stress paths in Fig. 3(c) have further evidenced the observations in Fig. 2. The mean effective stress p' undergoes an initial reduction to achieve the alleged phase transformation (PT) state (with the minimum p'), which signifies a temporary contraction behavior (Yang and Dai 2011; Dai et al. 2015, 2019). After the PT state, p' regains and increases with the increase of q, which refers to the dilation behavior. Also, the reduction degree of p' at the PT state, being 33.2%, is the largest for the specimen  $\sigma_r = 300 \text{ kPa}$ and the lowest for  $\sigma_r = 50$  kPa, being 1%. Despite the fact that the stress paths at large shear strains demonstrate a linear variation trend, they do not strictly fall on a unique line, especially for the case  $\sigma_r = 200 \text{ kPa}$ .

Fig. 4 presents the shear responses of rubber–sand mixtures with various rubber contents. In Fig. 4(a), the pure sand specimen exhibits a strain-softening behavior, and the deviatoric stress q is distinctly higher than other RSM specimens. With the increase of rubber content, q decreases and the shear response transforms into the mode of strain hardening. Zhou and Wang (2019) also found that the addition of rubber particles makes the stress–strain

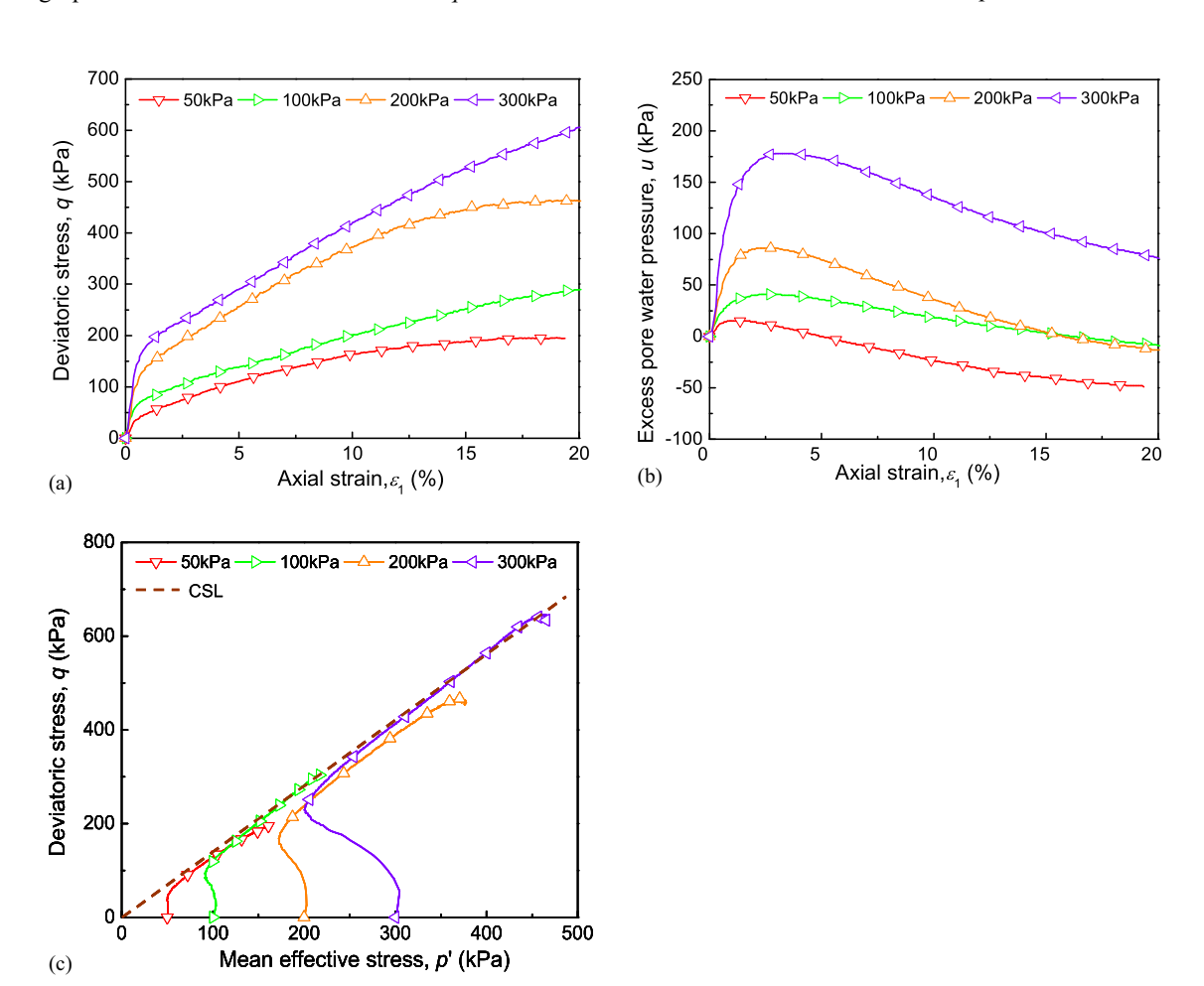


Fig. 3. Shear behavior of RSM samples with different confining pressures  $(D_r = 50\%, RC = 5\%)$ : (a) q versus  $\varepsilon_1$ ; (b) u versus  $\varepsilon_1$ ; and (c) q versus p'.

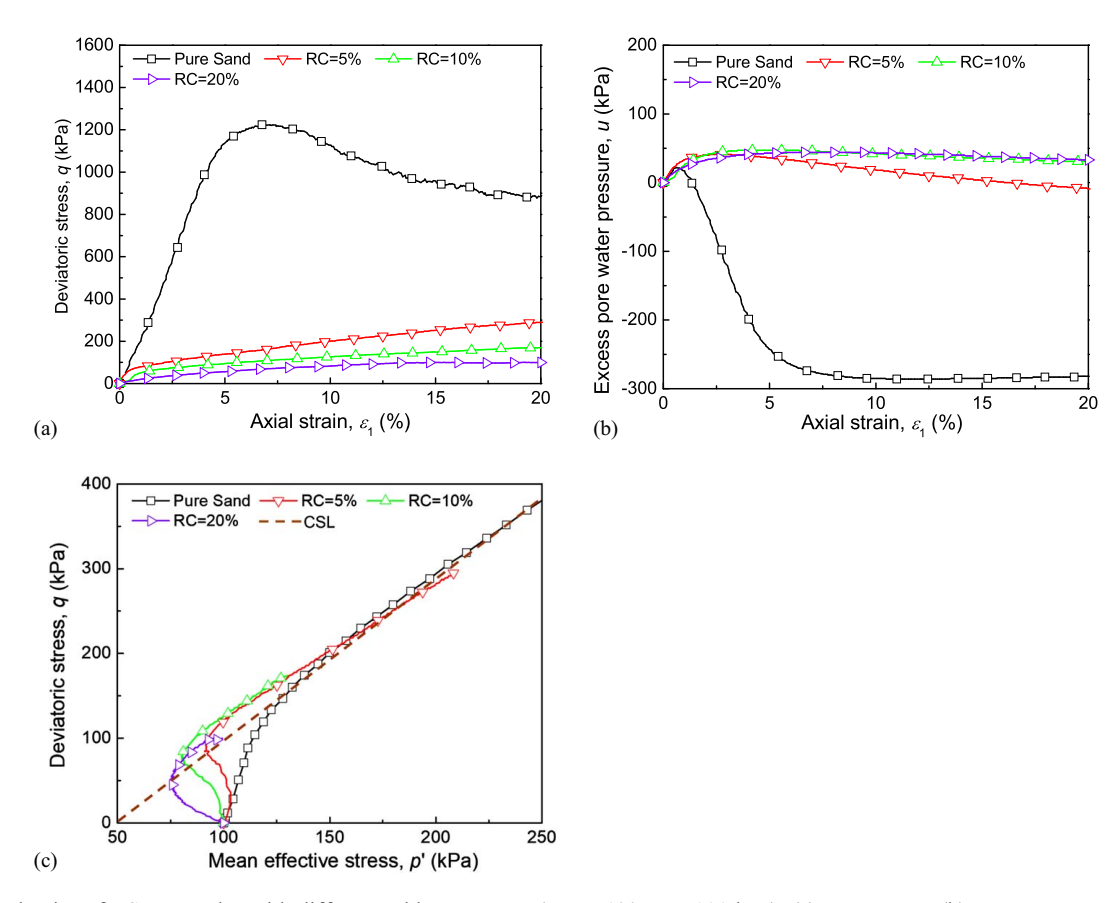
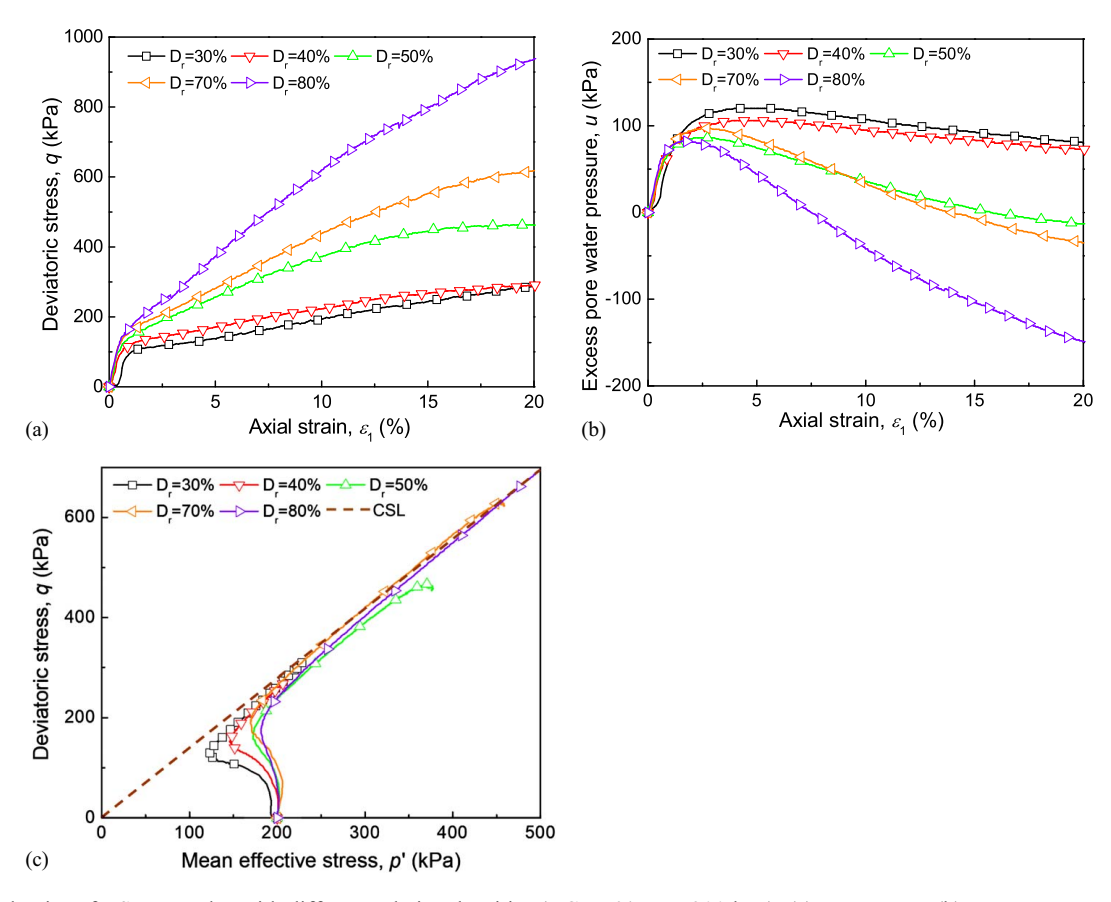
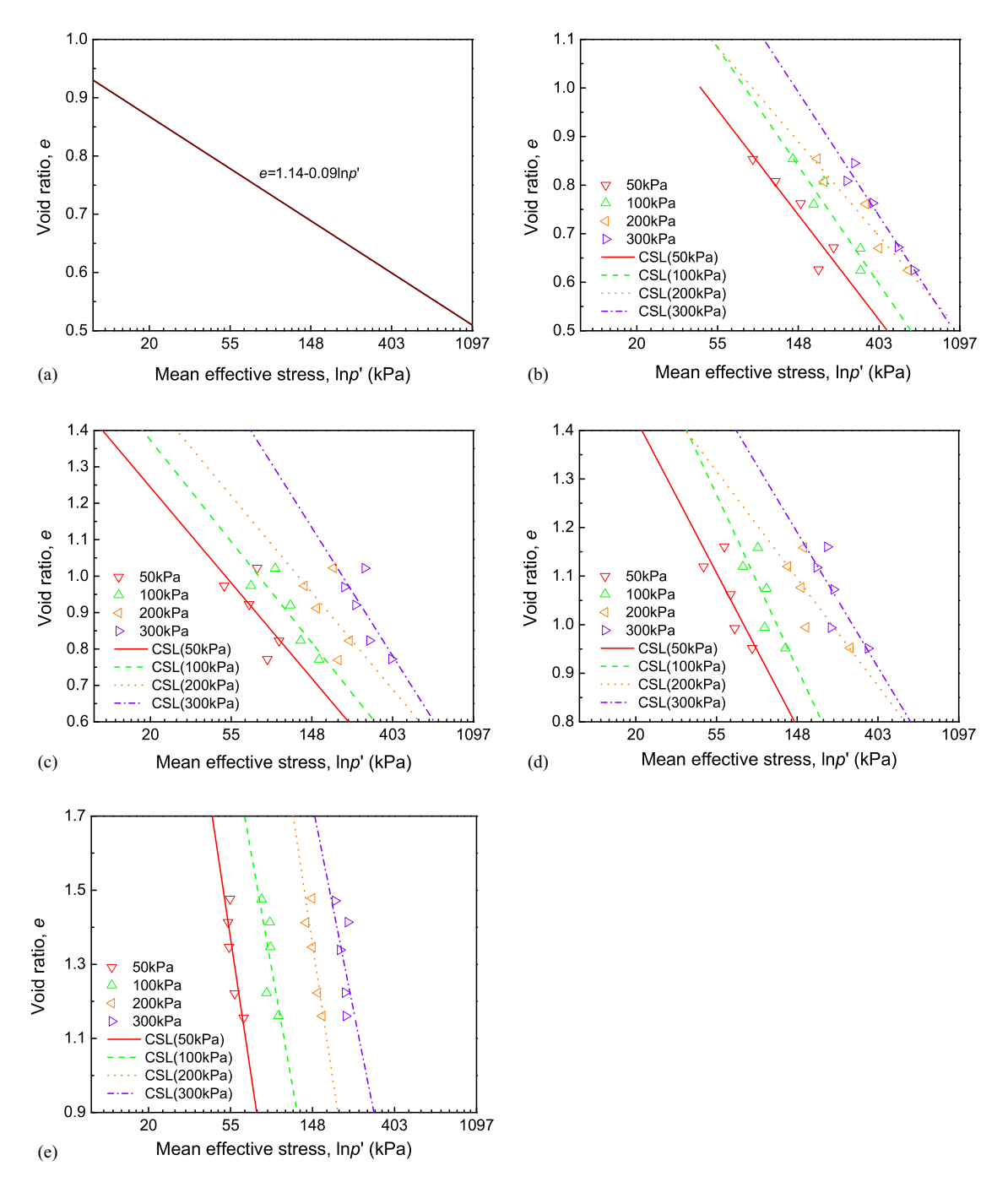


Fig. 4. Shear behavior of RSM samples with different rubber contents  $(D_r = 50\%, \sigma_r = 100 \text{ kPa})$ : (a) q versus  $\varepsilon_1$ ; (b) u versus  $\varepsilon_1$ ; and (c) q versus p'.



**Fig. 5.** Shear behavior of RSM samples with different relative densities (RC = 5%,  $\sigma_r$  = 200 kPa): (a) q versus  $\varepsilon_1$ ; (b) u versus  $\varepsilon_1$ ; and (c) q versus p'.



**Fig. 6.** Critical-state lines in e-lnp' space under various confining pressures: (a) pure sand; (b) RC = 5%; (c) RC = 10%; (d) RC = 15%; and (e) RC = 20%.

behavior of sands in the direct shear tests transit from the strain softening mode to the strain hardening mode, which may result from the enhancement of elasticity and compressibility with the presence of rubber particles between sand grains. Fig. 4(b) shows that the excess pore-water pressure of pure sand specimen decreases more rapidly than other RSM samples and maintains a significant negative value (around -300 kPa) at large shear strains. As seen from Fig. 4(c), the RSM specimens all display contraction behaviors at the early shearing stage and experience the PT state. It is also interesting to note that the stress ratio around the PT point is higher than the stress ratios at large shear strains for the RSM specimens, and they seem not to arrive at a common steady state. It is noted that the shear strength of sands is greatly reduced by

increasing the rubber content from 0% to 20%, and this result is different from the observation obtained by some previous researchers (Foose et al. 1996; Rao and Dutta 2006; Youwai and Bergado 2003).

Fig. 5 describes the shear behaviors of RSM specimens with different initial relative densities. Fig. 5(a) indicates that the increase of relative density leads to the promotion of both deviatoric stress and initial stiffness. In Fig. 5(b), the excess pore-water pressure is shown to first increase and then decrease as shearing goes on. Meanwhile, a higher relative density contributes to a lower excess pore-water pressure at the end of shearing, meaning that the RSM sample with a higher relative density is prone to more dilative responses. Similar results have been obtained in the consolidated

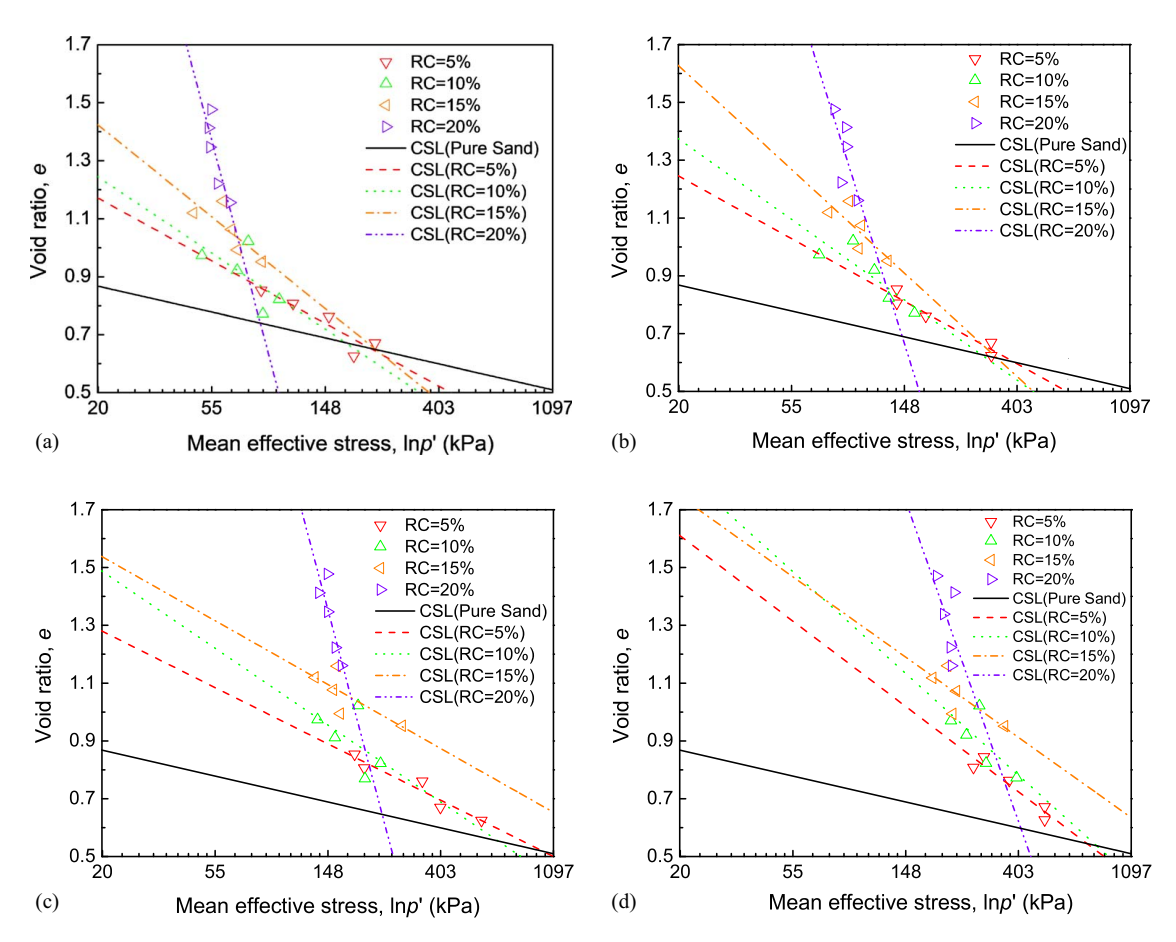


Fig. 7. Critical-state lines in e-lnp' space under various rubber contents: (a)  $\sigma_r = 50$  kPa; (b)  $\sigma_r = 100$  kPa; (c)  $\sigma_r = 200$  kPa; and (d)  $\sigma_r = 300$  kPa.

drained triaxial compression tests done by Zornberg et al. (2004) with respect to the RSM samples with the rubber content lower than 30%. The q-p' curves in Fig. 5(c) tend to approach a common line in the late stage of loading.

## **Critical States**

In critical-state soil mechanics (CSSM), the critical-state shear behavior is usually analyzed in e-lnp' and q-p' planes, although it can also be examined in a 3D space (Xiao et al. 2016, 2018 2019). The critical-state lines in e-lnp' and q-p' planes are characterized by the following two equations:

$$e = e_{\Gamma} - \lambda \ln p' \tag{1}$$

$$q = M p' \tag{2}$$

where q, p', and M= deviatoric stress, mean effective stress, and critical-state stress ratio, respectively; and  $e_{\Gamma}$ ,  $\lambda$  = void ratio at p' = 1 kPa, and the slope of the critical-state line in the e-lnp' plane.

Fig. 6 shows the critical-state lines in the e-lnp' plane. It should be noted that it is not easy for all specimens to rigorously reach the critical state with  $dq/d\varepsilon_q = dp'/d\varepsilon_q = d\varepsilon_v/d\varepsilon_q = 0$  ( $\varepsilon_v$  and  $\varepsilon_q$  are the volumetric and deviatoric strains, respectively). For a reasonable and consistent comparison analysis, we define the stress state at the critical state by averaging the stresses within the axial strain  $\varepsilon_1 = 15\%$ –20%. Given a specific rubber content, the position of CSL is pressure-dependent, and increasing the confining pressure tends to make the CSL shift (with the increase of  $e_\Gamma$ ) in the upper (or right) direction. Certainly, the CSLs at various confining pressures are not strictly parallel to each other. The critical-state shear

behavior of rubber-sand mixtures differs from that of pure sand, which has a unique critical-state line at various confining pressures in the e-lnp' plane. This is probably due to the fact that the rubber particles have greater compressibility than the sand particles; as the confining pressure increases, the pore volume gradually decreases, which is accompanied by a large volumetric compression for the rubber particles. Fig. 7 gives the critical-state lines in the e- $\ln p'$ plane for RSMs with different rubber contents. The rubber content has a great influence on the position of the critical-state line in the e-lnp' plane. It is seen that increasing the rubber content increases the slope  $\lambda$  of CSLs, meaning that RSMs with higher rubber contents have more pronounced compressibility. Interestingly, at the low-pressure condition (i.e.,  $\sigma_r = 50$  and 100 kPa), the CSL appears to rotate in the clockwise direction around a certain pivot point with the increase of rubber content if the case RC = 20% is excluded, whose  $\lambda$  value is far higher than other cases.

Further support for the observations from Figs. 6 and 7 is provided in Fig. 8, in which the slope of the critical-state line is compared at various confining pressures and rubber contents. It is shown in Fig. 8(a) that the slope  $\lambda$  increases with the increase of rubber content, irrespective of the pressure condition, and at a specific rubber content, it maintains to be almost the same with the variation of confining pressure, as indicated in Fig. 8(b). Even for the case RC = 20%,  $\lambda$  does not vary greatly with the confining pressure, and it is given to be  $\lambda = 1.29 \pm 0.18$ .

Fig. 9 compares the experimental results of this study with the findings in the literature in terms of the critical-state lines in the e-lnp' plane. It is seen that the observations in this study are to some extent consistent with the test results of Fu et al. (2017); that is,  $\lambda$  increases with the increase of rubber content, with the

0.0

(b)

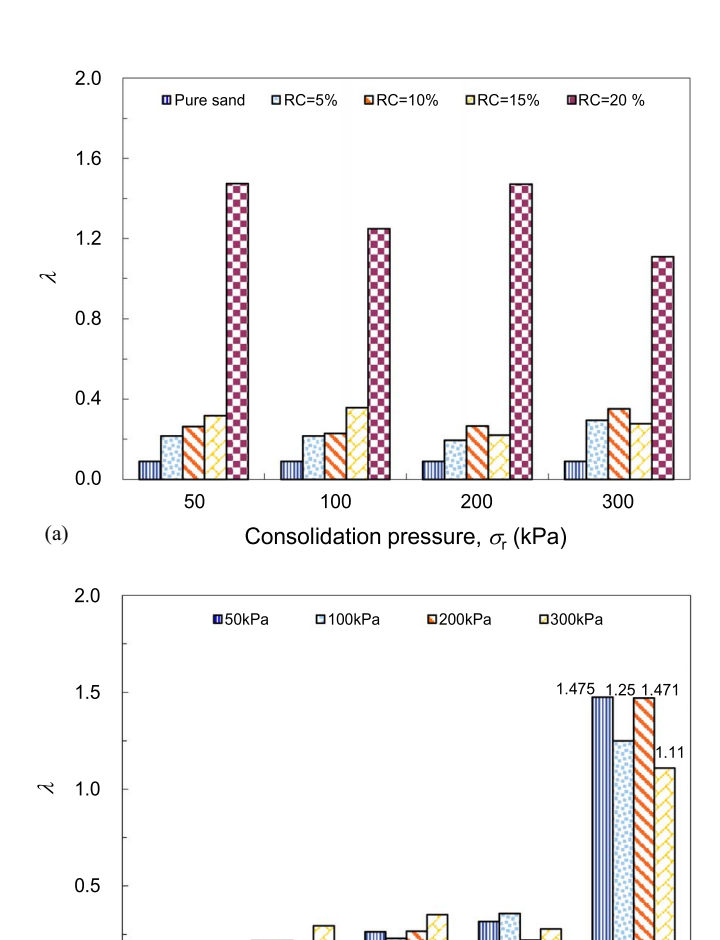


**Fig. 8.** Comparison of  $\lambda$  at (a) various rubber contents; and (b) various confining pressures.

10

Rubber content, RC (%)

15

20

5

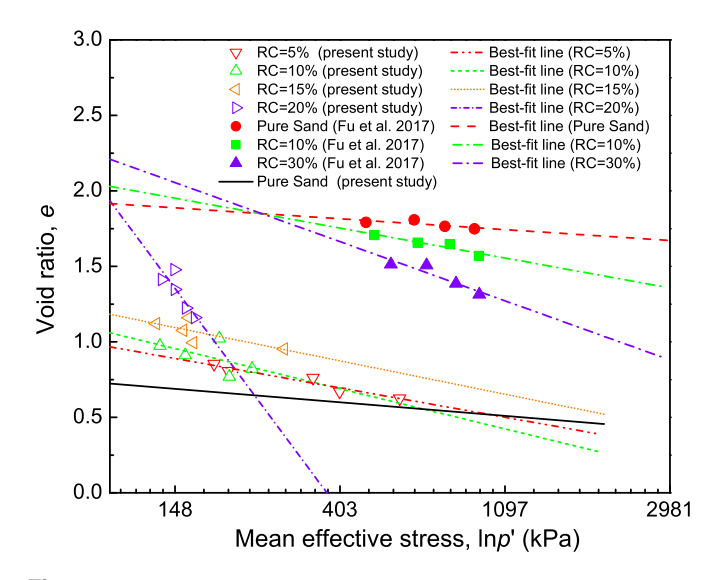


**Fig. 9.** Comparison of CSLs at various rubber contents ( $\sigma_r = 200 \text{ kPa}$ ).

critical-state line rotating in the clockwise direction. In general, the increase of rubber content promotes the compressibility of the RSM specimen and given a certain pressure variation, the corresponding void ratio variation is expected to be more significant at

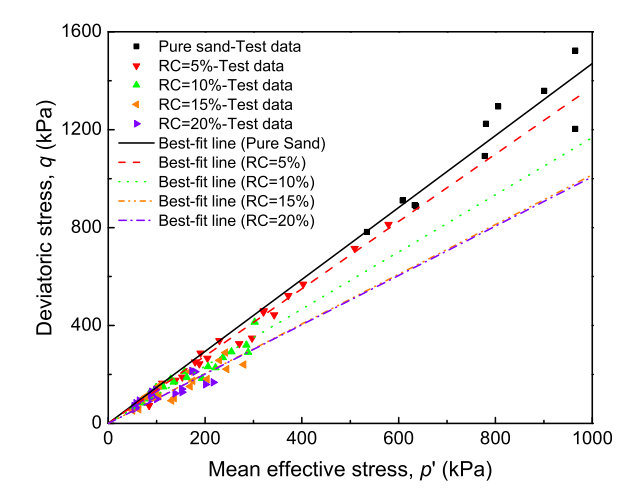


**Fig. 10.** Critical-state lines in the q-p' plane.

a relatively large rubber content. This is the primary reason why the slope  $\lambda$  increases with the increase of rubber content. However, there exists an obvious difference: the CSL obtained by Fu et al. (2017) seems to rotate around a fixed pivot point, whereas no fixed pivot point can be identified in the current study. Fig. 10 shows the critical-state lines in the q-p' plane for this study. It is clear that the slope M is the largest for the pure sand and reduces with the increase of rubber content. This is congruous to the finding from Fig. 4, in which the shear strength (i.e., the deviatoric stress) at large shear strains decreases with the increasing rubber content. Zhang et al. (2023) also concluded that adding rubber particles leads to a reduction of the slope M based on DEM simulations, and in their studies, the slope M gradually decreases from 1.24 to about 1.15 when the rubber content varies from 0% to 30%. Nevertheless, the variation of M is not remarkable at a relatively high rubber content, and the M values for the cases of RC = 15% and 20% are extremely close to each other.

## **Energy Analyses**

Given the conventional triaxial testing, the energy—work equation is given as follows (Dai and Yang 2017):

$$dW_{\text{input}} = p' d\varepsilon_{\nu} + q d\varepsilon_{q} = dE_{s} + dE_{d}$$
(3)

where  $\mathrm{d}\varepsilon_v$  and  $\mathrm{d}\varepsilon_q=$  volumetric and deviatoric strain increments at a loading step, respectively; and  $\mathrm{d}E_s$  and  $\mathrm{d}E_d=$  incremental strain energy (i.e., the incremental elastic potential energy stored in the specimen) and dissipated energy, respectively. For the undrained shear condition, the volumetric strain is regarded to be zero. In particular, the deviatoric strain  $\varepsilon_q$  is supposed to contain only the plastic part; that is,  $\varepsilon_q^e=0$ . Thus, Eq. (3) is rewritten as follows:

$$dW_{\text{input}} = qd\varepsilon_q = dE_v + dE_d = p'd\varepsilon_v^e + dE_d$$
 (4)

where  $dE_{\nu}$  (=  $p'd\varepsilon_{\nu}^{e}$ ) = incremental elastic volumetric strain energy; and  $d\varepsilon_{\nu}^{e}$  = incremental elastic volumetric strain, and it is given by the following equation:

$$\varepsilon_{\nu}^{e} = \frac{1 - 2\nu}{F} (\sigma_1 + \sigma_2 + \sigma_3) \tag{5}$$

For an estimation of the elastic volumetric strain energy, Young's modulus E is given by the initial tangential modulus obtained from the stress–strain curve, and an empirical expression proposed by Liu et al. (2017) is employed here to determine the

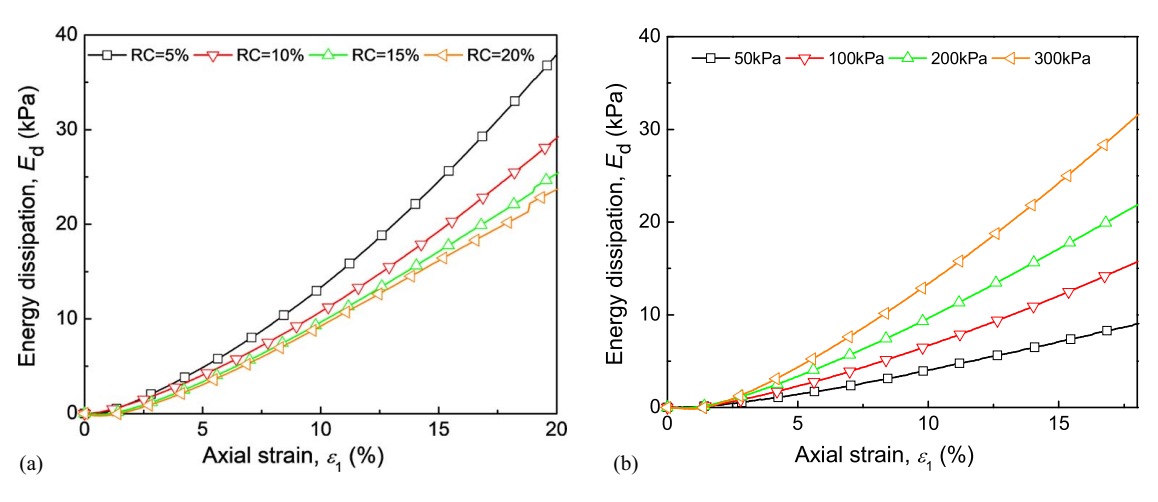


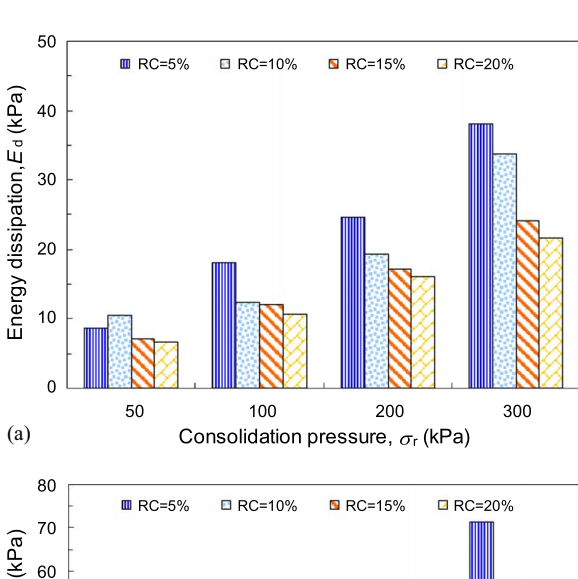
**Fig. 11.** Evolution of energy dissipation: (a)  $D_r = 30\%$ ,  $\sigma_r = 200$  kPa; and (b)  $D_r = 30\%$ , RC = 15%.

Poison's ratio v, which is written as follows:

$$\nu = 0.42 - 1.1RC \tag{6}$$

with the identification of the elastic volumetric strain energy and total work input, it is easy to figure out the energy dissipation during shear on the basis of Eq. (4). Fig. 11 presents the evolutions of the dissipated energy  $E_d$ , by focusing on two series of tests with different rubber content and consolidation pressures. It is natural that the energy dissipation increases with the axial strain due to the persistent work input during shear. With the promotion of rubber content, the dissipated energy, as shown in Fig. 11(a), decreases. This is probably ascribed to that the stress level at a high rubber content is lower than that at a low rubber content at a given pressure condition, which is also supported by the observation in Fig. 4. In this context, the contact force and energy dissipated through the interparticle friction behavior are expected to be lower at a higher rubber content, although the energy dissipation capacity of a specimen having more rubber particles is considered to be better due to that more rubber-rubber and rubber-sand contacts are in it. It should be mentioned that the interparticle friction coefficient for the rubber-rubber and rubber-sand contacts is generally higher than that for the sand-sand contacts. Fig. 11(b) shows that the energy dissipation at a fixed rubber content increases with the increase of confining pressures. This is also because the stress level during shear is relatively high at a large confining pressure condition, which leads to a more significant energy dissipation. In addition, a larger confining pressure also tends to help create more rubber-rubber and rubber-sand contacts, which could cause more energy dissipation. Fig. 12 gives further statistics of energy dissipation for the specimens with different confining pressures and rubber contents by considering two relative densities. Note that the accumulated energy dissipation is considered within the axial strain range of  $\varepsilon_1 = 0\%-15\%$ . One can have the same finding that the dissipated energy increases with the confining pressure but decreases with the rubber content.

Fig. 13 presents the evolution of volumetric strain energy  $E_{\nu}$  of RSM specimens. It is seen that  $E_{\nu}$  increases at first and then decreases with shear strain. Also, it keeps increasing with the increase of confining pressure and rubber content. Fig. 14 compares the volumetric strain energy for more RSM specimens, which further validates the observation in Fig. 13 that the volumetric strain energy is positively correlated with the confining pressure and rubber content. This may be because the increase of rubber content helps enhance the deformability of a specimen and thus promotes its



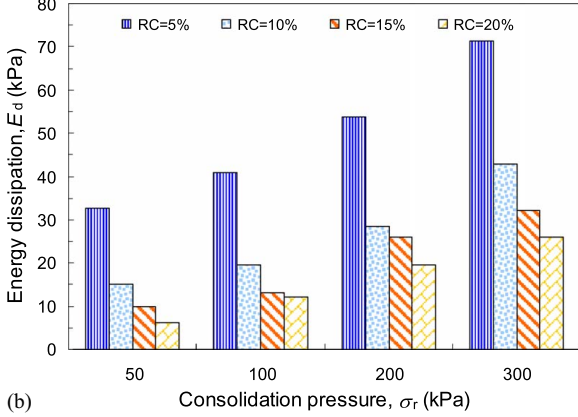


**Fig. 12.** Energy dissipation at various confining pressures and rubber contents: (a)  $D_r = 30\%$ ; and (b)  $D_r = 70\%$ .

capacity to store the elastic potential energy. Meanwhile, given a sample with a relatively high confining pressure, the stress level in it is anticipated to be comparatively high. In this regard, the volumetric strain energy rises with the increasing confining pressures. Despite all this, the value of volumetric strain energy  $E_{\nu}$ , as indicated in Figs. 13 and 14, is far less than the dissipated energy  $E_{d}$ , suggesting that the variation of the elastic potential energy stored in a specimen is limited at a given pressure condition and most input work is dissipated. Note that the volumetric strain energy in Fig. 14 is taken at the strain level of  $\varepsilon_1 = 15\%$ .

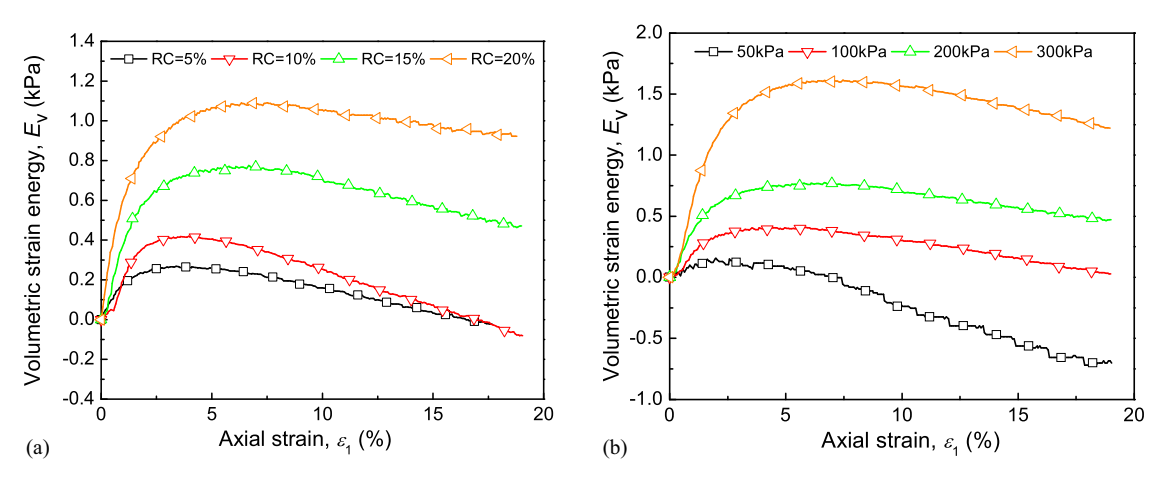
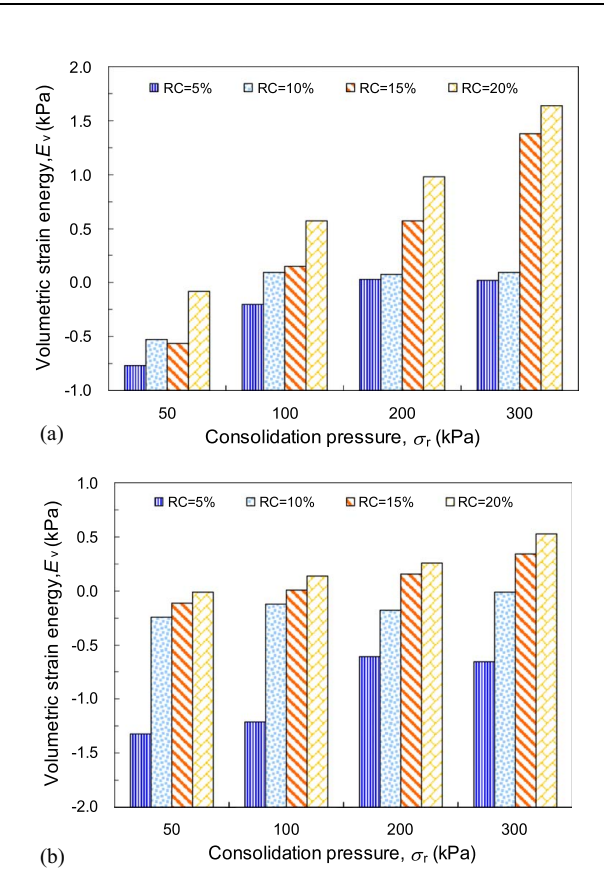


Fig. 13. Evolution of volumetric strain energy: (a)  $D_r = 30\%$ ,  $\sigma_r = 200$  kPa; and (b)  $D_r = 30\%$ , RC = 15%.



**Fig. 14.** Volumetric strain energy at various confining pressures and rubber contents: (a)  $D_r = 30\%$ ; and (b)  $D_r = 70\%$ .

#### **Conclusions**

A series of undrained triaxial tests are carried out to investigate the mechanical behavior of the rubber–sand mixtures, with a focus on the critical-state shear behavior and the mechanism of energy dissipation. The major findings are summarized as follows:

 The deviatoric stress q decreases with the increase of rubber content but increases with increasing confining pressures under otherwise similar conditions. A strain-softening behavior is observed for pure sand specimens, but a strain hardening behavior for RSM specimens. The excess pore-water pressure of pure sands decreases more rapidly than RSM specimens during the shear process. An increase of relative density leads to the

- promotion of the shear strength at failure, which is associated with a faster decrease of excess pore-water pressure. Under different confining pressures or rubber contents, the stress paths in the q-p' plane do not fall on a unique line at the late stage of shearing, but the stress paths for various relative densities seem to achieve a common steady state at the final shearing stage.
- 2. The position of the critical-state line in the e-lnp' plane depends on the confining pressure and rubber content. The increase of confining pressure makes the critical-state line shift toward the right (or upper) direction, with the slope  $\lambda$  not varying greatly. Increasing the rubber content makes the critical-state line rotate in the clockwise direction, with the slope  $\lambda$  increasing, and this rotation is not necessarily around a fixed pivot point. The slope M of the critical-state line in the q-p' plane reduces with the increase of rubber content, but this reduction trend becomes inconspicuous at a high rubber content level. The RSM specimens exhibit completely different critical-state shear behaviors compared with pure sands, which is related to the relatively high compressibility of rubber particles.
- 3. That the energy dissipation decreases with the increase of rubber content is linked with the reduction of stress level in the specimen, which decreases the contact force and the energy dissipation by means of the interparticle friction behaviors. The energy dissipation and volumetric strain energy both increase with the increase of confining pressure, and this can be accounted for by the increase of stress level, as well as the increase of the rubber-rubber and sand-rubber contacts, with the increasing confining pressure. The positive correlation of the volumetric strain energy with the rubber content is due to the fact that increasing the rubber content promotes the deformability of a specimen and thus enhances its capacity to store the elastic potential energy.

## **Data Availability Statement**

All data that support the findings of this study are available from the corresponding author upon reasonable request.

## **Acknowledgments**

This work is supported by the National Natural Science Foundation of China (Nos. 52078507 and 42071078) and the Science and Technology Program of Guangzhou City (No. 202002030195).

#### References

- Alimirzaei, S., M. Mohammadimehr, and A. Tounsi. 2019. "Nonlinear analysis of viscoelastic micro-composite beam with geometrical imperfection using FEM: MSGT electro-magneto-elastic bending, buckling and vibration solutions." Struct. Eng. Mech. 71 (5): 485–502.
- Anvari, S. M., I. Shooshpasha, and S. S. Kutanaei. 2017. "Effect of granulated rubber on shear strength of fine-grained sand." *J. Rock Mech. Geotech. Eng.* 9 (5): 936–944. https://doi.org/10.1016/j.jrmge.2017.03.008.
- Asadi, M., K. Thoeni, and A. Mahboubi. 2018. "An experimental and numerical study on the compressive behavior of sandrubber particle mixtures." *Comput. Geotech.* 104: 185–195. https://doi.org/10.1016/j.compgeo.2018.08.006.
- Bergado, D. T., S. Youwai, and A. Rittirong. 2005. "Strength and deformation characteristics of flat and cubical rubber tyre chip-sand mixtures." *Géotechnique* 55 (8): 603–606. https://doi.org/10.1680/geot.2005.55.8.603.
- Bernal-Sanchez, J., J. Mcdougall, D. Barreto, M. Miranda, and A. Marinelli. 2018. "Dynamic behaviour of shredded rubber soil mixtures." In Proc., 16th European Conf. on Earthquake Engineering. Thessaloniki, Greece: Springer.
- Bosscher, P. J., T. B. Edil, and S. Kuraoka. 1997. "Design of highway embankments using tire chips." *J. Geotech. Geoenviron. Eng.* 123 (4): 295–304. https://doi.org/10.1061/(ASCE)1090-0241(1997)123:4(295).
- Cheng, Z., J. Wang, and W. Li. 2020. "The micro-mechanical behaviour of sand–rubber mixtures under shear: An experimental study based on X-ray micro-tomography." Soils Found. 60: 1251–1268. https://doi. org/10.1016/j.sandf.2020.08.001.
- Cheung, G., and C. O'Sullivan. 2008. "Effective simulation of flexible lateral boundaries in two- and three-dimensional DEM simulations." *Particuology* 6 (6): 483–500. https://doi.org/10.1016/j.partic.2008.07.018.
- Dai, B., J. Yang, and X. Luo. 2015. "A numerical analysis of the shear behavior of granular soil with fines." *Particuology* 21 (4): 160–172. https://doi.org/10.1016/j.partic.2014.08.010.
- Dai, B.-B. 2018. "Influence of particle size and gradation on the stress-dilatancy behavior of granular materials during drained triaxial compression: Discussion." *Int. J. Geomech.* 18 (12): 07018018. https://doi.org/10.1061/(ASCE)GM.1943-5622.0001298.
- Dai, B.-B., Q. Liu, X. Mao, P.-Y. Li, and Z.-Z. Liang. 2023. "A reinterpretation of the mechanical behavior of rubber–sand mixtures in direct shear testing." *Constr. Build. Mater.* 363: 129771. https://doi.org/10.1016/j.conbuildmat.2022.129771.
- Dai, B.-B., and J. Yang. 2017. "Shear strength of assemblies of frictionless particles." *Int. J. Geomech.* 17 (11): 04017102. https://doi.org/10.1061 /(ASCE)GM.1943-5622.0001005.
- Dai, B. B., J. Yang, X. Q. Gu, and W. Zhang. 2019. "A numerical analysis of the equivalent skeleton void ratio for silty sand." *Geomech. Eng.* 17 (1): 19–30.
- Dai, B. B., J. Yang, and C. Y. Zhou. 2016. "Observed effects of interparticle friction and particle size on shear behavior of granular materials." Int. J. Geomech. 16 (1): 04015011. https://doi.org/10.1061/(ASCE)GM.1943-5622.0000520.
- Ding, Y., J. Zhang, X. Chen, X. Wang, and Y. Jia. 2021. "Experimental investigation on static and dynamic characteristics of granulated rubbersand mixtures as a new railway subgrade filler." *Constr. Build. Mater.* 273: 121955. https://doi.org/10.1016/j.conbuildmat.2020.121955.
- Fakharian, K., and A. Ahmad. 2021. "Effect of anisotropic consolidation and rubber content on dynamic parameters of granulated rubber–sand mixtures." Soil Dyn. Earthquake Eng. 141: 106531. https://doi.org/10 .1016/j.soildyn.2020.106531.
- Fonseca, J., A. Riaz, J. Bernal-Sanchez, D. Barreto Gonzalez, J. McDougall, M. Miranda Manzanares, and V. Dimitriadi. 2019. "Particle–scale interaction in sand–rubber mixtures and their influence on energy dissipation mechanisms." *Géotechnique Lett.* 9 (4): 1–6. https://doi.org/10.1680/jgele.18.00221.
- Foose, G. J., C. H. Benson, and P. J. Bosscher. 1996. "Sand reinforced with shredded waste tires." *J. Geotech. Eng.* 122 (9): 760–767. https://doi. org/10.1061/(ASCE)0733-9410(1996)122:9(760).

- Fu, R., M. R. Coop, and X. Q. Li. 2014. "The mechanics of a compressive sand mixed with tyre rubber." *Géotechnique Lett.* 4 (3): 238–243. https:// doi.org/10.1680/geolett.14.00027.
- Fu, R., M. R. Coop, and X. Q. Li. 2017. "Influence of particle type on the mechanics of sand–rubber mixtures." J. Geotech. Geoenviron. Eng. 143 (9): 04017059. https://doi.org/10.1061/(ASCE)GT.1943-5606 0001680
- Fu, R., B. Yang, X. Hu, B. Zhou, and M. R. Coop. 2023. "A micromechanical investigation of sand–rubber mixtures using the discrete element method." *Eng. Geol.* 318: 107106. https://doi.org/10.1016/j.enggeo 2023 107106
- Fuchiyama, M., M. Hyodo, Y. Nakata, N. Yoshimoto, and K. Imada. 2015.
  "Monotonic and cyclic shear behaviour of tire chips." In *Proc., Int. Symp. on Geomechanics from Micro to Macro (IS-Cambridge 2014)*, edited by K. Soga, K. Kumar, G. Biscontin, and M. Kuo. London: Taylor & Francis.
- Garga, V. K., and V. O'Shaughnessy. 2000. "Tire-reinforced earth-fill. Part
   1: Construction of a test fill, performance, and retaining wall design."
   Can. Geotech. J. 37 (1): 75–96. https://doi.org/10.1139/t99-084.
- Gu, X., M. Huang, and J. Qian. 2014. "DEM investigation on the evolution of microstructure in granular soils under shearing." *Granular Matter* 16 (1): 91–106. https://doi.org/10.1007/s10035-013-0467-z.
- Humphrey, D. N. 1999. "Civil engineering applications of tire shreds." In Proc., Tire Industry Conf. Hilton Head Island: Clemson University.
- Indraratna, B., Y. Qi, A. Heitor, and J. S. Vinod. 2019. "The influence of rubber crumbs on the critical state behavior of waste mixtures." E3S Web Conf. 92 (3): 06004. https://doi.org/10.1051/e3sconf/20199206004.
- Katiyar, V., A. Gupta, and A. Tounsi. 2022. "Microstructural/geometric imperfection sensitivity on the vibration response of geometrically discontinuous bi-directional functionally graded plates (2D-FGPs) with partial supports by using FEM." Steel Compos. Struct. 45 (5): 621–640.
- Kumar, Y., A. Gupta, and A. Tounsi. 2021. "Size-dependent vibration response of porous graded nanostructure with FEM and nonlocal continuum model." Adv. Nano Res. 11 (1): 1–17.
- Lee, J. H., R. Salgado, A. Bernal, and C. W. Lovell. 1999. "Shredded tires and rubber–sand as lightweight backfill." *J. Geotech. Geoenviron. Eng.* 125 (2): 132–141. https://doi.org/10.1061/(ASCE)1090-0241(1999) 125:2(132).
- Li, B., M. Huang, and X. Zeng. 2016. "Dynamic behavior and liquefaction analysis of recycled-rubber sand mixtures." J. Mater. Civ. Eng. 28 (11): 04016122. https://doi.org/10.1061/(ASCE)MT.1943-5533.0001629.
- Li, W., C. Y. Kwok, C. S. Sandeep, and K. Senetakis. 2019. "Sand type effect on the behaviour of sand-granulated rubber mixtures: Integrated study from micro- to macro-scales." *Powder Technol.* 342: 907–916. https://doi.org/10.1016/j.powtec.2018.10.025.
- Liu, F. C., M. T. Wu, N. Liu, Y. F. Zhang, and J. L. Chen. 2017. "Experimental study on Poisson's ratio of rubber–sand mixtures." [In Chinese.] Chin. J. Rock Mech. Eng. 36 (S01): 3596–3606.
- Liu, L., G. Cai, and S. Liu. 2018. "Compression properties and micromechanisms of rubber-sand particle mixtures considering grain breakage." Constr. Build. Mater. 187: 1061–1072. https://doi.org/10.1016/j .conbuildmat.2018.08.051.
- Lopera Perez, J. C., C. Y. Kwok, and K. Senetakis. 2016. "Effect of rubber size on the behaviour of sand–rubber mixtures: A numerical investigation." *Comput. Geotech.* 80: 199–214. https://doi.org/10.1016/j.compgeo.2016.07.005.
- Lopera Perez, J. C., C. Y. Kwok, and K. Senetakis. 2017. "Micromechanical analyses of the effect of rubber size and content on sand–rubber mixtures at the critical state." *Geotext. Geomembr*. 45: 81–97. https://doi.org/10.1016/j.geotexmem.2016.11.005.
- Muraro, S., and C. Jommi. 2019. "Implication of end restraint in triaxial tests on the derivation of stress-dilatancy rule for soils having high compressibility." Can. Geotech. J. 56 (6): 840–851. https://doi.org/10.1139 /cgj-2018-0343.
- Nakhaei, A., S. M. Marandi, S. Sani Kermani, and M. H. Bagheripour. 2012. "Dynamic properties of granular soils mixed with granulated rubber." Soil Dyn. Earthquake Eng. 43: 124–132. https://doi.org/10.1016/j .soildyn.2012.07.026.
- Pistolas, G. A., A. Anastasiadis, and K. Pitilakis. 2018. "Dynamic behaviour of granular soil materials mixed with granulated rubber: Effect of

- rubber content and granularity on the small-strain shear modulus and damping ratio." *Geotech. Geol. Eng.* 36: 1267–1281.
- Qi, Y., B. Indraratna, and M. R. Coop. 2019. "Predicted behavior of saturated granular waste blended with rubber crumbs." *Int. J. Geomech.* 19 (8): 04019079. https://doi.org/10.1061/(ASCE)GM.1943-5622.0001440.
- Rao, G. V., and R. K. Dutta. 2006. "Compressibility and strength behaviour of sand–tyre chip mixtures." *Geotech. Geol. Eng.* 24: 711–724. https:// doi.org/10.1007/s10706-004-4006-x.
- Sarajpoor, S., A. Kavand, P. Zogh, and A. Ghalandarzadeh. 2020. "Dynamic behavior of sand–rubber mixtures based on hollow cylinder tests." *Constr. Build. Mater.* 251: 118948. https://doi.org/10.1016/j .conbuildmat.2020.118948.
- Senthen Amuthan, M., A. Boominathan, and S. Banerjee. 2020. "Undrained cyclic responses of granulated rubber–sand mixtures." Soils Found. 60: 871–885. https://doi.org/10.1016/j.sandf.2020.06.007.
- Shariatmadari, N., M. Karimpour-Fard, and A. Shargh. 2018. "Undrained monotonic and cyclic behavior of sand–ground rubber mixtures." *Earthquake Eng. Eng. Vibr.* 17 (3): 541–553. https://doi.org/10.1007/s11803-018-0461-x.
- Tabrizi, M. K., S. Abrishami, E. S. Hosseininia, S. Sharifi, and S. Ghorbani. 2019. "Experimental investigation on the behavior of fine-grained soils containing waste rubber tires under repeated and static loading using direct shear apparatus." *Constr. Build. Mater.* 223: 106–119. https://doi .org/10.1016/j.conbuildmat.2019.06.159.
- Tsang, H.-H., S. H. Lo, X. Xu, and M. Sheikh. 2012. "Seismic isolation for low-to-medium-rise buildings using granulated rubber–soil mixtures: Numerical study." *Earthquake Eng. Struct. Dyn.* 41 (14): 2009–2024. https://doi.org/10.1002/eqe.2171.
- Wu, M., W. Tian, F. Liu, and J. Yang. 2023. "Dynamic behavior of geocell-reinforced rubber sand mixtures under cyclic simple shear loading." Soil Dyn. Earthquake Eng. 164: 107595. https://doi.org/10.1016/j.soildyn.2022.107595.
- Wu, Q., W. j. Ma, Q. Liu, K. Zhao, and G. Chen. 2021. "Dynamic shear modulus and damping ratio of rubber–sand mixtures with a wide

- range of rubber content." *Mater. Today Commun.* 27: 102341. https://doi.org/10.1016/j.mtcomm.2021.102341.
- Xiao, Y., H. Liu, X. Ding, Y. Chen, J. Jiang, and W. Zhang. 2016. "Influence of particle breakage on critical state line of rockfill material." *Int. J. Geomech.* 16 (1): 04015031. https://doi.org/10.1061/(ASCE)GM .1943-5622.0000538.
- Xiao, Y., L. Long, T. Matthew Evans, H. Zhou, H. Liu, and A. W. Stuedlein. 2019. "Effect of particle shape on stress-dilatancy responses of medium-dense sands." *J. Geotech. Geoenviron. Eng.* 145 (2): 04018105. https://doi.org/10.1061/(ASCE)GT.1943-5606.0001994.
- Xiao, Y., A. W. Stuedlein, Q. Chen, H. Liu, and P. Liu. 2018. "Stress-strain-strength response and ductility of gravels improved by polyurethane foam adhesive." *J. Geotech. Geoenviron. Eng.* 144 (2): 04017108. https://doi.org/10.1061/(ASCE)GT.1943-5606 .0001812.
- Yang, J., and B. B. Dai. 2011. "Is the quasi-steady state a real behaviour? A micromechanical perspective." *Géotechnique* 61 (2): 175–183. https://doi.org/10.1680/geot.8.P.129.
- Yang, J., and X. D. Luo. 2018. "The critical state friction angle of granular materials: Does it depend on grading?" *Acta Geotech.* 13: 535–547. https://doi.org/10.1007/s11440-017-0581-x.
- Youwai, S., and D. T. Bergado. 2003. "Strength and deformation characteristics of shredded rubber tire—sand mixtures." *Can. Geotech. J.* 40 (2): 254–264. https://doi.org/10.1139/t02-104.
- Zhang, J.-Q., X. Wang, and Z.-Y. Yin. 2023. "DEM-based study on the mechanical behaviors of sand–rubber mixture in critical state." *Constr. Build. Mater.* 370: 130603. https://doi.org/10.1016/j.conbuildmat.2023.130603.
- Zhou, E. Q., and Q. Wang. 2019. "Experimental investigation on shear strength and liquefaction potential of rubber–sand mixtures." Adv. Civ. Eng. 2019: 5934961.
- Zornberg, J. G., A. R. Cabral, and C. Viratjandr. 2004. "Behaviour of tire shred–sand mixtures." *Can. Geotech. J.* 41 (2): 227–241. https://doi.org/10.1139/t03-086.